Oxygen-Vacancy Complex in Silicon .2. O-17 Electron-Nuclear Double-Resonance

Vankemp, R.; Sprenger, M.; Sieverts, E.G.; Ammerlaan, C.A.J.

DOI
10.1103/PhysRevB.40.4054

Publication date
1989

Published in
Physical Review. B, Condensed Matter

Oxygen-vacancy complex in silicon. II. ^{17}O electron-nuclear double resonance

R. van Kemp, M. Sprenger, E. G. Sieverts, and C. A. J. Ammerlaan
Natuurkundig Laboratorium der Universiteit van Amsterdam, Valckenierstraat 65, NL-1018 XE Amsterdam, The Netherlands
(Received 10 March 1989)

An electron-nuclear double-resonance (ENDOR) study was performed on the negatively charged oxygen-vacancy complex in silicon. By introducing the isotope ^{17}O (nuclear spin $I=\frac{5}{2}$) to an enrichment of about 40%, it was possible to detect ENDOR transitions of this nucleus. In the experiment the magnetic hyperfine interaction with the unpaired defect electron and the nuclear quadrupole interaction were measured. The anisotropic hyperfine interaction could be described by a small allowed admixture of p orbitals. In such a simple one-electron description the Fermi-contact interaction could not satisfactorily be understood. The quadrupole interaction could be explained as arising mainly from unbalanced charges in the oxygen p orbital that points in the direction of the silicon neighbors with which a Si-O-Si "molecule" is formed. The technique of field-swept ENDOR was used to determine the relative signs of the hyperfine- and quadrupole-interaction constants. The strong interference of the two interactions gives rise to the occurrence of forbidden EPR transitions and a very complicated angular dependence of the ENDOR frequencies upon rotation of the magnetic field. As a consequence, for some orientations no ENDOR was observed at all.

I. INTRODUCTION

The negatively charged state of the oxygen-vacancy complex in silicon, also called the Si-A center, was one of the first defects that was observed with EPR (electron paramagnetic resonance) in silicon that was irradiated at room temperature with electrons at energies of 0.5–1.5 MeV.[1,2] The EPR spectrum was labeled $B1$.[3] It was noticed that the defect was produced only in n-type, quartz-crucible-grown silicon upon irradiation at room temperature. The defect was not observed at all, or with very low intensities, in float-zone silicon, which is known to have an oxygen concentration that is a few orders of magnitude lower, nor was it seen in p-type or high-resistivity n-type silicon. In crucible-grown, n-type material irradiated at low temperatures (below 20 K), the center was only detected after annealing at temperatures higher than about 77 K. In connection with the defect, an electron-acceptor level at $E_c-0.17$ eV was found.[4]

The above observations led to a model in which the defect is formed by an interstitial oxygen atom which traps a vacancy produced during the irradiation.[1] Vacancies are known to be mobile in n-type silicon at temperatures above 77 K. The model as shown in Fig. 1 was further confirmed in studies by Watkins and Corbett[5] and by Corbett *et al.*[6] In Ref. 5 an extensive study of the defect by EPR was presented. A linear combination of atomic orbitals (LCAO) analysis of the observed hyperfine interactions with ^{29}Si nuclei surrounding the defect was given, as well as the activation energies for thermally activated electronic and for stress-induced atomic reorientation of the defect. In Ref. 6 infrared-absorption studies in correlation with EPR measurements were presented. Both macroscopic (production rate) and microscopic (stress-induced alignment) evidence for the identification of the 12-μm infrared-absorption band with the defect was given. This 12-μm band (836 cm^{-1}) appears upon irradiation and is thought to be the equivalent of the 9-μm (1136-cm^{-1}) infrared-absorption band, which is ascribed to the antisymmetric stretch vibration mode of isolated interstitial oxygen in the distorted bond-centered position between two silicon atoms.[7]

With electron-nuclear double resonance (ENDOR), a detailed study has been made of hyperfine interactions with ^{29}Si nuclei in the surrounding crystal lattice.[8,9] From this experiment, it was concluded that the electronic structure of the defect was highly similar to that of the negative vacancy.[10]

Up to now, the presence of oxygen in a radiation defect in silicon has been inferred from ^{17}O hyperfine interactions only in the EPR spectrum labeled Si-SL1.[11,12] This spectrum is generally ascribed to an excited $S=1$ triplet state of the neutral charge state of the oxygen-vacancy complex. However, there is only indirect evidence that the spectra $B1$ and SL1 belong to different charge states of the same defect. From spectrum $B1$, no direct experimental proof for the presence of oxygen has been reported yet. In general, EPR and ENDOR are very suitable methods to provide such conclusive evidence. However, a high enough concentration in the isotope ^{17}O with nuclear spin $I=\frac{5}{2}$ (natural abundance 0.037%) is needed. Moreover, in EPR the hyperfine structure can easily be obscured by more or less resolved hyperfine interactions with ^{29}Si nuclei. When $A(^{17}O)<12$ MHz this will certainly be the case, and one must expect the hyperfine interaction to be rather small as the oxygen nucleus lies on the twofold axis of the defect, where a contact hyperfine interaction is symmetry forbidden.[8] An attempt by Watkins and Corbett[5] to observe the oxygen hyperfine interaction in a sample that had been enriched to approximately 1.5% in the isotope ^{17}O failed.

In Sec. II we will give an outline of our sample preparation and measuring techniques; in Sec. III we present our experimental results, and in Sec. IV the interpretation of the measured hyperfine and quadrupole in-

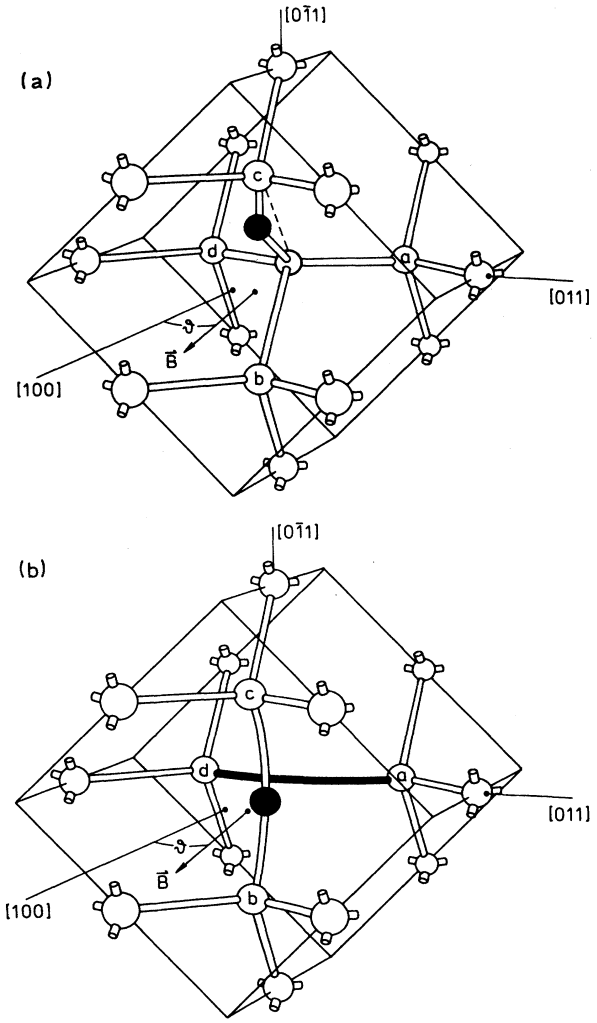

FIG. 1. Model of oxygen (solid sphere) in silicon, (a) before and (b) after electron irradiation. The oxygen-vacancy complex in (b) is shown in orientation *ad*, in which the defect electron is mainly localized in the reconstructed bond between the atoms *a* and *d*. All further data refer to this standard orientation *ad*.

teractions are discussed in relation with the established model for the defect.

II. EXPERIMENT

The major problem in this study was to obtain a high enrichment in the ^{17}O isotope in silicon. A method used by Muller[13] consisted of oxidation of the silicon samples by heating them for 24 h at 1000 °C in a quartz ampoule containing a few milligrams of water enriched with 10% $H_2{}^{17}O$. After subsequent diffusion at 1390 °C for 2 weeks, the final ^{17}O content appeared to be reduced to about 3% of the total oxygen concentration. This rather dramatic decrease is probably caused by the exchange with the oxygen isotope ^{16}O (natural abundance 99.759%) from the quartz ampoules during the oxidation and the diffusion. It is difficult to circumvent this problem, as quartz is the only suitable material that can be used for the ampoule in which the diffusion takes place. During the process, the quartz is at the same high temperature as the silicon and can easily undergo reactions.

This problem was solved by using an infrared-radiation oven (Quad Elliptical Radiant Heating Chamber, model E4-10, manufactured by Research Inc.). In this type of oven the samples are placed in one of the two foci of an elliptical mirror. In the other focus a quartz radiation lamp is placed. In this oven four such lamps and mirrors surround the sample. With this heating system the quartz ampoule stays at much lower temperatures. Placing the samples on silicon supports prevents every direct contact with the quartz. The samples were heated for 10 d at 1390 °C in an oxygen atmosphere enriched to 52.3% in the isotope ^{17}O. As the samples need not be quenched extremely rapidly, it was sufficient to turn off the lamps after completion of the diffusion process. The final enrichment in the isotope ^{17}O was about 40%, as determined from the optical absorption in the 9-μm band.[14]

The electron irradiations were carried out with a Van de Graaff electrostatic accelerator at energies of about 1.5 MeV and currents on the order of 7 μA cm^{-2}. During the irradiations, the samples were mounted on a copper block that was tightly fixed inside a holder with a water-cooled mantle. Care was taken to keep the temperature of the sample below ~70 °C during the irradiations. The production of the oxygen-vacancy complex was monitored by EPR and resistivity measurements using the four-point-probe technique.

The silicon we used for the diffusion was *n*-type, P-doped, float-zone material with a phosphorus concentration of about 9×10^{17} atoms cm^{-3}. As the oxygen and phosphorus concentrations are of the same order, phosphorus-vacancy complexes and other phosphorus-related defects[15,16] are also produced during the irradiations, as well as divacancies. Consequently, the production of oxygen-vacancy complexes is smaller. However, we made use of the fact that O-V^- has a higher annealing temperature (~450 °C) than all other defects. By a 20-min anneal at 220 °C, all the complexes dissociate, leaving only O-V^-. A side effect of such an anneal is that the vacancies that are released can again be trapped by the remaining "free" interstitial oxygen atoms. The sequence irradiation-annealing was thus repeated a few times until the intensity of the $B1$ spectrum did not increase any more.

The ENDOR measurements were performed using a superheterodyne *K*-band spectrometer. To do nuclear magnetic resonance (NMR) and EPR simultaneously, a cylindrical TE_{011} resonance cavity made of Epibond was used. The inner wall is covered with a thin layer of silver in which a spiral groove is cut, thus enabling the wall to act as a coil for radiofrequency currents.[17] NMR transitions were recorded as a change in the intensity of the dispersion component of the EPR signal. We used double phase-sensitive detection. To this end the magnetic field was sine-wave modulated at 83.3 Hz and the radiofrequency signal was on-off modulated at a frequency of 3.3 Hz. The magnetic field **B** was rotated in a {110} plane of the crystal. The measurements were done with the sample at a temperature of ~25 K.

TABLE I. Electron g tensor ($\overleftrightarrow{g}$) and hyperfine- ($\overleftrightarrow{A}$) and quadrupole- ($\overleftrightarrow{Q}$) interaction tensor parameters for the oxygen-vacancy complex. Units of hyperfine and quadrupole parameters are kHz; the absolute error is 4 kHz. The error in the g values is ±0.0001. The tensor components are given in Cartesian coordinates by the tensors $\overleftrightarrow{T}$; also given are the principal values T_i—$i=1,2,3$—for the tensors on their own principal axes $\mathbf{n}_i$.

Tensor	$\overleftrightarrow{T}$			i	T_i	$\mathbf{n}_i$
$\overleftrightarrow{g}$	2.0033	0	0	1	2.0033	[100]
	0	2.0059	−0.0034	2	2.0025	[011]
	0	−0.0034	2.0059	3	2.0093	[0$\bar{1}$1]
$\overleftrightarrow{A}$	4362.8	0	0	1	4362.8	[100]
	0	2297.9	−3294.7	2	−996.7	[011]
	0	−3294.7	2297.9	3	5592.6	[0$\bar{1}$1]
$\overleftrightarrow{Q}$	149.3	0	0	1	149.3	[100]
	0	−74.6	248.3	2	173.7	[011]
	0	248.3	−74.6	3	−323.0	[0$\bar{1}$1]

III. EXPERIMENTAL RESULTS

A. EPR spectrum

Figure 2 shows the angular variation of the EPR spectrum for rotation of the magnetic field in the (0$\bar{1}$1) plane. This dependence can be analyzed with the spin Hamiltonian

$$\mathcal{H}=\mu_B\mathbf{B}\cdot\overleftrightarrow{g}\cdot\mathbf{S}\ , \tag{1}$$

with $S=\frac{1}{2}$. The $\overleftrightarrow{g}$ tensor is constrained by the symmetry of the defect, in this case rhombic I (point group $2mm$), and can be written as

$$\overleftrightarrow{g}=\begin{bmatrix} g_{xx} & 0 & 0 \\ 0 & g_{zz} & g_{yz} \\ 0 & g_{yz} & g_{zz} \end{bmatrix}\ . \tag{2}$$

The values of the $\overleftrightarrow{g}$-tensor elements were determined by making a computer fit to Eq. (1). They are given in Table I. The principal values $g_1=2.0033\pm0.0001$ ($\|[100]$), $g_2=2.0025\pm0.0001$ ($\|[011]$), and $g_3=2.0093\pm0.0001$ ($\|[0\bar{1}1]$) are in good agreement with Ref. 5.

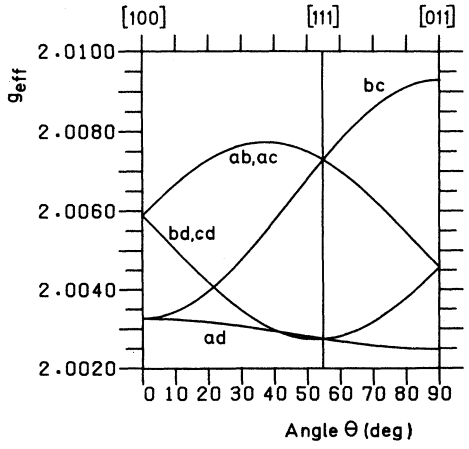

FIG. 2. Angular dependence of the effective g values, g_{eff}, of the Si-$B1$ EPR spectrum for the magnetic field rotating in the (0$\bar{1}$1) plane. The labels of the orientations correspond to Fig. 1(b).

When a ^{17}O nucleus is incorporated in the defect, the EPR measurements can be described with the spin Hamiltonian

$$\mathcal{H}=\mu_B\mathbf{B}\cdot\overleftrightarrow{g}\cdot\mathbf{S}-g_N\mu_N\mathbf{B}\cdot\mathbf{I}+\mathbf{S}\cdot\overleftrightarrow{A}\cdot\mathbf{I}+\mathbf{I}\cdot\overleftrightarrow{Q}\cdot\mathbf{I}\ , \tag{3}$$

with $S=\frac{1}{2}$ and $I=\frac{5}{2}$. To the electron Zeeman-interaction term in Eq. (1) are added the nuclear Zeeman interaction, the interaction of the defect electron with the ^{17}O nucleus, and the nuclear quadrupole interaction, respectively. The hyperfine-interaction tensor and the quadrupole-interaction tensor can be written as

$$\overleftrightarrow{A}=\begin{bmatrix} A_{xx} & 0 & 0 \\ 0 & A_{zz} & A_{yz} \\ 0 & A_{yz} & A_{zz} \end{bmatrix}$$

and (4)

$$\overleftrightarrow{Q}=\begin{bmatrix} Q_{xx} & 0 & 0 \\ 0 & -\frac{1}{2}Q_{xx} & Q_{yz} \\ 0 & Q_{yz} & -\frac{1}{2}Q_{xx} \end{bmatrix}\ ,$$

reflecting the point-group symmetry of the defect.

In Fig. 3 the EPR line for the orientation bc with the magnetic field $\mathbf{B}$ parallel to the [011] direction is shown (a) for a sample containing ^{16}O-V^-, and (b) for a sample also with ^{17}O-V^-. In Fig. 3(b) we have also represented by bars the positions of the ^{17}O hyperfine lines as calculated using the spin Hamiltonian (3) and the values of $\overleftrightarrow{A}$ and $\overleftrightarrow{Q}$ as determined with ENDOR, to be discussed in Sec. III B. It is seen that the apparent relative intensity of two of the ^{29}Si hyperfine satellites has changed due to the presence of the ^{17}O hyperfine lines.

Inspection of Fig. 3 shows that it is impossible to determine the hyperfine interaction for ^{17}O from EPR, all the more so because this was the only direction for which the ^{17}O hyperfine interaction could be discerned at all. Therefore ENDOR experiments were indispensable because they have a resolving power that is about 3 orders of magnitude higher than that of EPR.

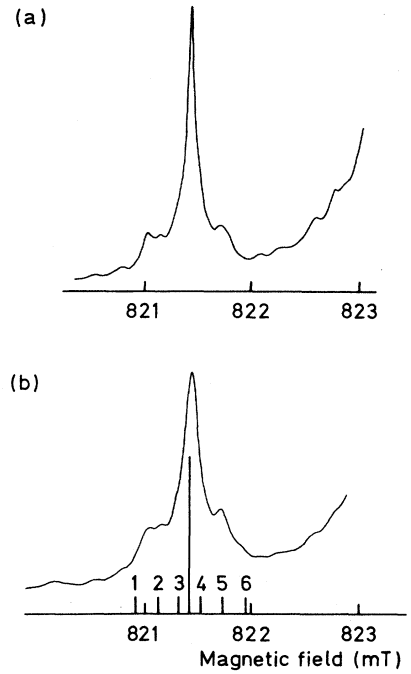

FIG. 3. EPR spectrum of O-V^- for orientation *bc* with B||[011]. (a) For a sample with natural oxygen; (b) for a sample enriched to about 40% in ^{17}O. Calculated positions and relative intensities of the ^{17}O hyperfine lines are indicated. Numbers refer to EPR transitions which belong to the following nuclear-spin states: 1, $m_I=+\frac{5}{2}$; 2, $m_I=+\frac{3}{2}$; 3, $m_I=+\frac{1}{2}$; 4, $m_I=-\frac{1}{2}$; 5, $m_I=-\frac{3}{2}$; 6, $m_I=-\frac{5}{2}$. The relative intensity change between the two ^{29}Si hyperfine satellites at the left of the central line is just visible.

B. ENDOR spectrum

The ^{17}O ENDOR experiments were carried out after having completed the ^{29}Si ENDOR measurements.[8,9] It turned out that it was of crucial importance to know the exact position of the ^{29}Si ENDOR lines in order to recognize the oxygen ENDOR. The ENDOR measurements of ^{17}O can be described with the spin Hamiltonian given in Eq. (3). To first order, the solution of this equation is

$$E=g_{\rm eff}\mu_B m_S B-g_N\mu_N m_I B+m_S m_I A_{\rm eff}+(m_I^2-\tfrac{35}{12})Q_{\rm eff}\ . \tag{5}$$

From Eq. (5) it follows that the frequencies at which ENDOR transitions ($\Delta m_S=0$ and $\Delta m_I=1$) will occur are given by

$$\begin{aligned}\nu&=|\nu_z\pm\tfrac{1}{2}A_{\rm eff}/h\pm 4Q_{\rm eff}/h|\ ,\\ \nu&=|\nu_z\pm\tfrac{1}{2}A_{\rm eff}/h\pm 2Q_{\rm eff}/h|\ ,\\ \nu&=|\nu_z\pm\tfrac{1}{2}A_{\rm eff}/h|\ ,\end{aligned} \tag{6}$$

where $\nu_z=-g_N\mu_N B/h$ is the nuclear Zeeman frequency, with $g_N\mu_N/h=-5.772$ MHz T^{-1} for ^{17}O.[18] The plus and minus signs are uncorrelated, thus giving rise to two groups of five equally spaced lines, the spacing between the lines in a group being $2Q_{\rm eff}/h$. In this experiment the first-order solution of Eq. (3) turned out not to give a sufficiently accurate approximation to the measured hyperfine and quadrupole interactions. The deviations from the equal spacing were very large for some directions.

It turned out that the intensities of the ENDOR lines decreased rapidly when the magnetic field was rotated out of the [100] and [011] directions along which the principal axes of the *g* tensor lie. In the experiment, ENDOR lines from the EPR orientations *ad* and *bc* were only observed between [100] and about [100]+10° (one transition of orientation *bc* could be observed up to [100]+53°), and between [011] and about [011]−35°. ENDOR frequencies for the orientations *ab*,*ac* and *bd*,*cd* were not even observed at all. As a full rotation pattern always strongly overdetermines the spin-Hamiltonian parameters, the observed experimental data were already sufficient to completely determine them. Changes in the transition probabilities when the magnetic field is rotated out of the principal directions of the *g* tensor could indeed be calculated.

A computer fit to the spin-Hamiltonian equation (3) was made to determine the hyperfine and quadrupole tensor elements. In this fit the $\overleftrightarrow{g}$-tensor elements and the nuclear *g* factor were kept constant. Only frequencies that were measured in the [100] and [011] directions on the EPR orientations *ad* and *bc* were used in the fit. Results are shown in Table I. Subsequently, simulations were made which indeed reproduced the measured frequencies outside the [100] and [011] directions within the error margin of 4 kHz, as given in Table I. From field-swept ENDOR (FSE) measurements the relative signs of the tensor elements of $\overleftrightarrow{A}$ and $\overleftrightarrow{Q}$ were determined.[19] FSE also helped in assigning observed lines in the [100] direction to particular nuclear transitions in a stage in which all ENDOR lines had not yet been recognized.

Figure 4 shows the complete angular dependence of the ENDOR frequencies as calculated upon rotation of the magnetic field in the $(0\bar{1}1)$ plane. As can be seen, the pattern is very complicated and the curves exhibit strong departures from the normally observed $\cos(2\theta)$ patterns. The 20 branches of the orientations *ad* and *bc* have been marked in the figure.

IV. INTERPRETATION OF EXPERIMENTAL RESULTS

A. Hyperfine-interaction tensor $\overleftrightarrow{A}$

The hyperfine interaction with the ^{17}O nucleus mainly arises from unpaired electronic spin density in the oxygen orbitals. This density can be described by a wave function which is a linear combination of atomic orbitals (LCAO). For the purpose of the analysis, the hyperfine-interaction tensor $\overleftrightarrow{A}$ is decomposed into isotropic and traceless anisotropic parts:

$$\overleftrightarrow{A}=a\overleftrightarrow{1}+\overleftrightarrow{B}\ . \tag{7}$$

The isotropic Fermi-contact term

$$a=\tfrac{2}{3}\mu_0 g\mu_B g_N\mu_N\eta^2\alpha^2|\Psi(0)|_s^2 \tag{8}$$

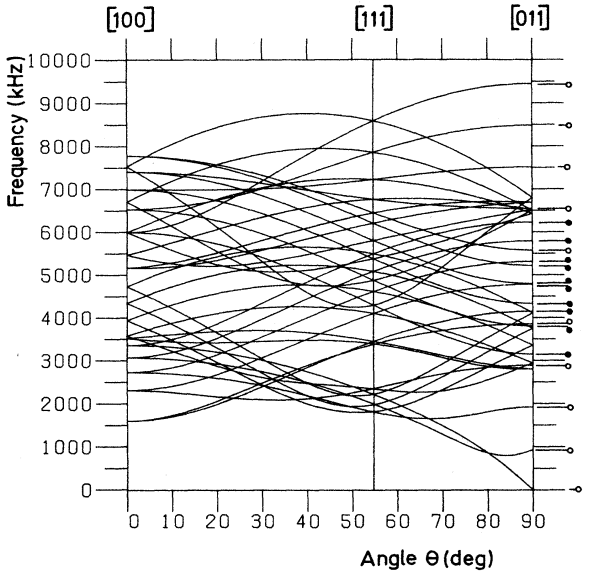

FIG. 4. Angular dependence of the ENDOR frequencies for rotation of the magnetic field **B** in the (0$\bar{1}$1) plane. The frequencies found for the EPR orientations *bc* and *ad* are indicated: ○ denotes orientation *bc* and ● denotes orientation *ad*. Note that the frequency scale is absolute. The microwave frequency was 22.9713 GHz.

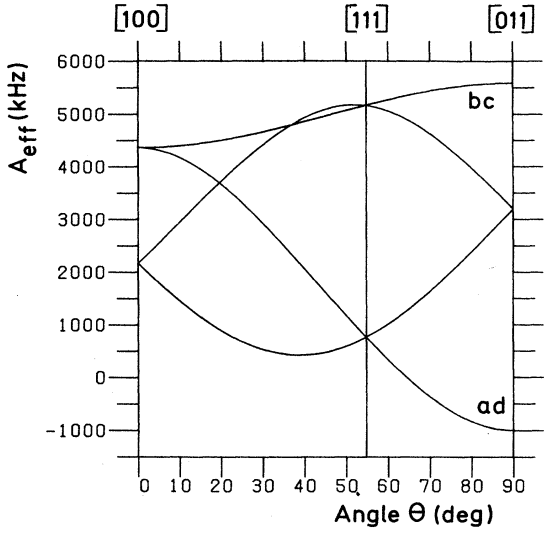

FIG. 5. Angular dependence of the effective A values, A_{eff}, for rotation of the magnetic field **B** in the (0$\bar{1}$1) plane. Orientations *bc* and *ad* are indicated.

is related to spin density in the oxygen s orbitals. The anisotropic part arises from dipole-dipole interaction with spins in the p orbitals. It leads to a tensor with the form

$$\vec{\vec{B}} = \begin{bmatrix} 2b & 0 & 0 \\ 0 & -b & 0 \\ 0 & 0 & -b \end{bmatrix}, \tag{9}$$

with

$$b = (\mu_0/4\pi) g \mu_B g_N \mu_N \tfrac{2}{5} \eta^2 \beta^2 \langle r^{-3} \rangle_p \ . \tag{10}$$

The parameters η, α, and β are the coefficients in the LCAO expansion; α^2 and β^2 are a measure for the amount of s and p character of the wave function, respectively, and η^2 measures the localization of the wave function on the oxygen nucleus. The atomic-orbital parameters $|\Psi(0)|_s^2$ and $\langle r^{-3} \rangle_p$ can, for instance, be found as a result of theoretical calculations.[20] Equations (7) and (9) represent an axially symmetric tensor. However, for this defect with rhombic I symmetry, axiality is not symmetry required. In order to include the deviations from axial behavior, the principal values of the hyperfine-interaction tensor $\vec{\vec{A}}$ are written as $a+2b$, $a-b+c$, and $a-b-c$, where c is a measure for the deviation from axiality. In Table II results of the analysis are given. The table includes values for a/b, a measure for the anisotropy, and b/c, a measure for the "axiality" of the tensor.

In Fig. 5 we show an angular plot of the effective A values. From this figure, or alternatively from the numerical values given in Table I, it is concluded that the $\vec{\vec{A}}$ tensor is to a good approximation axial around the [011] direction. This can be understood from the one-electron model proposed by Watkins and Corbett.[5] According to this model, the paramagnetic electron occupies an antibonding b_1 state. For an atom that lies on the twofold axis of the defect, the only allowed LCAO orbital centered at such an atom is $p_y + p_z$, as it has to be antisymmetric with respect to reflection about the (011) mirror plane. A p orbital with $\eta^2 = 100\%$ would give an axial hyperfine-interaction tensor with $b = -168.4$ MHz.[20] Thus a localization of only 1.18% can already account for the axial part of the observed dipole-dipole interaction tensor.

The deviation from axiality should then be explained

TABLE II. Reduced hyperfine parameters a, b, c, a/b, b/c, and reduced quadrupole parameters q, r, and q/r. The spin and charge localization, η^2 and ϵ^2, respectively, were calculated with the atomic wave-function parameter $\langle r^{-3} \rangle_p = 39.31$ Å^{-3} from Ref. 18.

Tensor	a (kHz)	b (kHz)	c (kHz)	a/b	b/c	α^2 (%)	β^2 (%)	η^2 (%)
$\vec{\vec{A}}$	2986.3	−1991.5	−614.9	−1.50	3.24	0	100	1.18
		q (kHz)	r (kHz)		$\lvert q/r \rvert$			ϵ^2 (%)
$\vec{\vec{Q}}$		−161.5	12.2		13.2			23

by other effects like the dipole-dipole interaction between the ^{17}O nucleus and the unpaired spin at the atoms a at $[\bar{1}\,1\,1]$ and d at $[\bar{1}\,\bar{1}\,\bar{1}]$. We calculated this interaction for various ^{17}O-atom positions on the [100] axis through the defect. The diagonalized tensor for the interaction between a nucleus and an electron spin in a point charge reads

$$\overleftrightarrow{B}=\begin{bmatrix} 2b_{dd} & 0 & 0 \\ 0 & -b_{dd} & 0 \\ 0 & 0 & -b_{dd} \end{bmatrix}, \tag{11}$$

where $b_{dd}=(\mu_0/4\pi)g\mu_B g_N \mu_N \eta^2 (1/R^3)$, η^2 is the amount of unpaired electron, and R is the distance between the point charge and the nucleus. This tensor is axially symmetric parallel to the direction between the point charge and the nucleus.

In order to calculate the dipole-dipole tensor, it is necessary to know the position of the oxygen nucleus along the positive x axis. Infrared studies by Bosomworth *et al.*[21] for the interstitial oxygen and the oxygen-vacancy complex indicated an angle between the Si(b)—O—Si(c) bonds of $2\alpha \sim 160°$, corresponding to a position of the oxygen atom of about [0.75,0,0], i.e., a displacement of 1.02 Å. From a theoretical study of neutral substitutional oxygen by DeLeo *et al.*,[22] a displacement of 1.0–1.1 Å was found. A theoretical study of the neutral oxygen-vacancy complex in an excited state by Canuto and Fazzio[23] gave a displacement of 1.1 Å. This corresponds to the position [0.81,0,0] and an angle $2\alpha = 164.8°$.

In Table III the results are given of calculations with an unpaired spin density corresponding to 0.3 electron on each of the atoms a and d.[5,8] The table includes the hyperfine-tensor values measured in the experiment, the results of the calculations with the contributions of sites a and d added, and the experimental values after correction for the distant dipole-dipole interactions. In the calculations the spin densities at the atoms a and d are either considered as point charges (pc), or are distributed in Slater-type orbitals (orb) centered at these sites. The Slater-type orbitals have the form

$$\chi_{3s,j}=\frac{N_s}{\sqrt{4\pi}} r_j^2 \exp\left[-\alpha_s \frac{r_j}{a_0}\right],$$
$$\chi_{3p_x,j}=N_p \frac{\sqrt{3}}{\sqrt{4\pi}} x_j r_j \exp\left[-\alpha_p \frac{r_j}{a_0}\right], \tag{12}$$

and similar expressions for $\chi_{3p_y,j}$ and $\chi_{3p_z,j}$ with $j=a,d$. The coefficients N_s and N_p are given by normalization requirements: $N_s^2=(2\alpha_s/a_0)^7/6!$ and $N_p^2=(2\alpha_p/a_0)^7/6!$, where a_0 is the Bohr radius; the Slater-orbital exponents α_s and α_p are dimensionless parameters and are chosen to have the values $\alpha_s=1.87$ and $\alpha_p=1.60$. The integration over these orbitals is easy when using the polynomial expressions derived by Ammerlaan and Wolfrat.[24] In Table III the values b, the spin densities η^2 [derived from Eqs. (9) and (10), assuming $\beta^2=1$], and the deviations from axiality, $|b/c|$, are also shown.

As can be seen from the quotient $|b/c|$, the tensor becomes more axial after subtraction of the distant dipole-dipole contributions. The marked difference between calculations in the point-charge and Slater-orbital approximations shows that the results depend sensitively on the exact spatial extent of the wave function centered at atoms a and d, as these are so close to the oxygen atom. After subtraction of $\overleftrightarrow{B}_{pc}$, the dipole-dipole tensor becomes only slightly more axial; after subtraction of $\overleftrightarrow{B}_{orb}$, the axiality is much better. Apparently, point charges are much too localized. Also, Slater-type orbitals tend to be so, although they give already much better results. In view of this trend, we conclude that the deviation from [011] axiality can be explained from distant dipole-dipole contributions. The results do not depend sensitively on the position of the oxygen atom on the [100] axis, although the smaller distortion away from the vacancy site is favored.

TABLE III. Calculated dipole-dipole tensors and results after subtraction from the experimental tensor. pc labels the values calculated for point charges at the positions of atoms a and d; orb labels the values calculated for Slater-type orbitals centered at the positions of the point charges. B_1, B_2, and B_3 are principal values. Units of B_i and b are kHz.

	B_1 ‖[100]	B_2 ‖[011]	B_3 ‖[0$\bar{1}$1]	b	$\lvert b/c\rvert$	η^2 (%)
$\overleftrightarrow{B}_{expt}$	1376.6	−3983.0	2606.4	−1991.5	3.2	1.18
^{17}O at [0.75,0,0]						
$\overleftrightarrow{B}_{orb}$	−387.6	−9.8	397.4			
$\overleftrightarrow{B}_{pc}$	−183.8	−41.7	225.5			
$\overleftrightarrow{B}_{expt}-\overleftrightarrow{B}_{orb}$	1764.2	−3973.2	2209.0	−1986.6	8.9	1.18
$\overleftrightarrow{B}_{expt}-\overleftrightarrow{B}_{pc}$	1560.4	−3941.3	2380.9	−1970.7	4.8	1.17
^{17}O at [0.81,0,0]						
$\overleftrightarrow{B}_{orb}$	−378.6	10.2	368.4			
$\overleftrightarrow{B}_{pc}$	−182.8	−29.1	211.9			
$\overleftrightarrow{B}_{expt}-\overleftrightarrow{B}_{orb}$	1755.2	−3993.2	2238.0	−1996.6	8.3	1.19
$\overleftrightarrow{B}_{expt}-\overleftrightarrow{B}_{pc}$	1559.4	−3953.9	2394.5	−1977.0	4.7	1.17

is favored.

We also conclude that the successful interpretation of the hyperfine-interaction constants b and c confirms the sign of these parameters, thereby eliminating the ambiguity left by the analysis of the experimental data. The signs of all elements of the $\overleftrightarrow{A}$ and $\overleftrightarrow{Q}$ tensors are thus as given in Table I. The one-electron LCAO model requires the Fermi-contact interaction with nuclei on the [100] axis to be zero, in conflict with the experimental finding. In addition, in the LCAO model the parameters a and b should have the same (negative) signs, whereas in the experiment they are found to have opposite signs. One must conclude that the one-electron LCAO model does not appropriately account for the isotropic hyperfine interaction. In this respect it is relevant to note that, when applying Eq. (8), the measured value for this interaction, $a=+2986.3$ kHz, corresponds to a core polarization $|\Psi_\uparrow|_s^2-|\Psi_\downarrow|_s^2$ of only 0.06% of an electron, though of the opposite sign. A possible qualitative explanation of the Fermi-contact interaction is the mechanism of exchange core polarization (ECP). One can distinguish two types of ECP. First, a direct mechanism in which the $1s$ and $2s$ electrons of the oxygen are spin polarized by the unpaired defect electron. Second, an indirect mechanism in which the unpaired electron polarizes the paired Si orbitals, whereas these polarized Si cores, in turn, overlap the oxygen cores and produce a net spin density at the oxygen nucleus. Calculations that take into account these effects have been made to explain the negative and positive Fermi-contact interactions observed in some color centers like F_2^- in LiF, where the fluorine ions also lie in a nodal plane of the electron wave function.[25]

A second possibility that can be considered is the effect of many-electron interactions. This mechanism was studied quantitatively by Lannoo[26] for the negative vacancy in silicon. Exactly the same symmetry considerations as for O-V^- apply to this defect, yet contact interactions with ^{29}Si nuclei that lie in the (011) mirror plane of the defect were observed. The conclusion of Lannoo is that the contact term, of which he considered the largest one, with $a=2105.8$ kHz,[10,27] can be explained by many-electron effects. As the total electronic structure of the oxygen-vacancy complex and the negative vacancy are very similar,[8,9] the calculations of Lannoo indicate that many-electron effects should also be important in this case. Unfortunately, detailed calculations for O-V^- do not exist. Therefore, predictions about the sign of a are also lacking.

B. Quadrupole-interaction tensor $\overleftrightarrow{Q}$

The nuclear quadrupole interaction arises from the interaction between the nuclear quadrupole moment and the electric field gradient at the site of the nucleus,

$$Q_{ij}=\frac{eQ}{2I(2I-1)}\frac{\partial^2 V}{\partial x_i \partial x_j}\ , \tag{13}$$

where Q is the nuclear quadrupole moment, I is the nuclear spin, and V the electrostatic potential.[28] For ^{17}O, the nuclear moment equals $Q=-2.6\times10^{-30}$ m^2.[18]

The quadrupole interaction is a measure for the unbalanced charge density in the $2p$ orbitals of the oxygen atom. This interaction can be regarded as the equivalent of the hyperfine interaction, which measures the unbalanced spin density near the nucleus.

Besides the effect of charge in the oxygen $2p$ orbitals, distant charges, such as those on atoms a and d, can also cause a field gradient. The field gradient at the site of the oxygen nucleus, due to a point charge $-e$ of one electron located at a site at distance R, gives an axially symmetric quadrupole tensor with principal values $(2q,-q,-q)$, where

$$q=-\frac{1}{4\pi\epsilon_0}\frac{e^2Q}{2I(2I-1)}\frac{1}{R^3}\ . \tag{14}$$

As the exact position of the oxygen nucleus is not known, we have calculated this tensor for several positions along the positive [100] direction. For the oxygen nucleus at [0.75,0,0] and point charges $-0.3e$ at the sites a, $[\bar{1}\,1\,1]$, and d, $[\bar{1}\,\bar{1}\,\bar{1}]$, one finds a quadrupole tensor with principal values $Q_1^{pc}=+0.8$ kHz ($\|[100]$), $Q_2^{pc}=+0.2$ kHz ($\|[011]$), and $Q_3^{pc}=-1.0$ kHz ($\|[0\bar{1}1]$). It is clear that the contribution due to the field gradient from the distant point charges cannot, by far, explain the experimentally observed quadrupole interaction as given in Table I. Stated differently, the quadrupole interaction must be due almost entirely to p orbitals of the oxygen atom itself.

A p orbital gives rise to an axially symmetric quadrupole tensor with principal values $(2q,-q,-q)$, where

$$q=-\frac{1}{4\pi\epsilon_0}\frac{e^2Q}{2I(2I-1)}\tfrac{2}{5}\langle r^{-3}\rangle_p\ . \tag{15}$$

For a filled oxygen $2p$ orbital, for which $\langle r^{-3}\rangle_p=39.27\times10^{30}$ m^{-3},[20] this results in $q=+710.1$ kHz. From the measured hyperfine interaction, it has been calculated that an unpaired-spin (us) density of 1.18% of an electron is present at the ^{17}O nucleus in a $2p$ orbital parallel to the [011] direction. This will give a quadrupole interaction tensor $\overleftrightarrow{Q}^{us}$ with principal values $Q_1^{us}=+16.8$ kHz ($\|[011]$), $Q_2^{us}=-8.4$ kHz ($\|[100]$), and $Q_3^{us}=-8.4$ kHz ($\|[0\bar{1}1]$). It is obvious that this mechanism cannot explain the measured quadrupole interaction either.

The experimental quadrupole tensor is, to a good approximation, axial, parallel to $[0\bar{1}1]$, i.e., along the line that connects the atoms b and c in Fig. 1(b), and perpendicular to the axis of the $\overleftrightarrow{A}$ tensor. Principal values of the $\overleftrightarrow{Q}$ tensor can be written as $(2q,-q+r,-q-r)$, in which the deviation from axiality is given by r. We find $|q|=161.5$ kHz and $|r|=12.2$ kHz; the ratio $|q/r|=13.2$ as a measure for the axiality indicates that the deviation is rather small. $\overleftrightarrow{Q}^{pc}$ and $\overleftrightarrow{Q}^{us}$ are contributions from the observed unpaired-spin densities. If we subtract them as known contributions from the measured quadrupole-interaction tensor, we arrive at a tensor $\overleftrightarrow{Q}$ with principal values $Q_1=+156.9$ kHz ($\|[100]$), $Q_2=+156.7$ kHz ($\|[011]$), and $Q_3=-313.6$ kHz ($\|[0\bar{1}1]$). This results in $q=-156.8$ kHz and $r=+0.1$ kHz. The deviation from axiality has strongly decreased ($|q/r|\approx1568$), while q has hardly changed. The axial direction is still along the line that connects atoms b and c in Fig. 1(b).

For the bonding of the oxygen atom between the silicon atoms, a simple molecular-orbital picture can be given. In view of the near linearity of the Si(b)—O—Si(c) structure, this bonding can be achieved by two sp-hybridized orbitals on the oxygen along the [0$\bar{1}$1] direction. The remaining four oxygen valence electrons can be accommodated pairwise in $2p$ orbitals perpendicular to [0$\bar{1}$1]. Due to the hybridization, a full $2p$ electron along [0$\bar{1}$1] would be lacking from a spatially balanced $(2p)^6$ configuration. From the calculated and measured quadrupole interactions, an electron deficiency of $\epsilon^2=22\%$ along [0$\bar{1}$1] can be derived. The difference between the expected 100% and the observed 22% electron deficiency can be explained by the following mechanisms.

(1) The Si(b)—O—Si(c) structure is not linear, but makes an angle of $\sim 160°$. This would reduce the expected electron deficiency only to 90%. At the same time, however, the axiality should become worse ($q/r \sim 3.5$).

(2) Oxygen is strongly electronegative, so that charge in the Si—O bond will be drawn towards the oxygen nucleus. This will make its distance r to the oxygen nucleus smaller and, consequently, increase $\langle r^{-3} \rangle_p$ for the electrons in these Si—O bonds. The effective field gradient, due to the total charge distribution, will be reduced in this way, as will the quadrupolar interaction, as is measured. This effect can be of considerable magnitude. According to Pauling,[29] the ionicity of a single bond is

$$f_i = 1 - \exp[-(X_A - X_B)^2/4] , \quad (16)$$

where $X_A - X_B$ is the difference in electronegativity between atoms A and B. For the Si—O bond, $X_A - X_B = 1.7$,[29] giving $f_i = 0.51$. This should be compared with a typical ionic bond as Na—Cl, where $f_i = 0.67$. One should be aware that the value 0.51 is only approximative, partly because the structure which we consider is more complicated. Still, this simple calculation indicates that the strong electronegativity of oxygen can be responsible for a considerable reduction of the electron deficiency in the p orbital along the [0$\bar{1}$1] direction. The observed negative sign of the principal value along the axial direction of the Si(b)—O—Si(c) structure is consistent with this model.

ACKNOWLEDGMENTS

We would like to thank T. Gregorkiewicz and H. Schlatter for developing the ^{17}O-diffusion procedure. The discussions with A. B. van Oosten were very clarifying. This work received financial support from the Foundation for Fundamental Research on Matter (FOM).

[1] G. Bemski, J. Appl. Phys. **30**, 1195 (1959).
[2] G. D. Watkins, J. W. Corbett, and R. M. Walker, J. Appl. Phys. **30**, 1198 (1959).
[3] G. D. Watkins, in *Radiation Damage in Semiconductors,* edited by P. Baruch (Dunod, Paris, 1965), p. 97.
[4] G. K. Wertheim, Phys. Rev. **105**, 1730 (1957); **110**, 1272 (1958).
[5] G. D. Watkins and J. W. Corbett, Phys. Rev. **121**, 1001 (1961).
[6] J. W. Corbett, G. D. Watkins, R. M. Chrenko, and R. S. McDonald, Phys. Rev. **121**, 1015 (1961).
[7] W. Kaiser, P. H. Keck, and C. F. Lange, Phys. Rev. **101**, 1264 (1956).
[8] R. van Kemp, E. G. Sieverts, and C. A. J. Ammerlaan, this issue, the preceding paper, Phys. Rev. B **40**, 4037 (1989).
[9] R. van Kemp, E. G. Sieverts, and C. A. J. Ammerlaan, Mater. Sci. Forum **10-12**, 875 (1986).
[10] M. Sprenger, S. H. Muller, E. G. Sieverts, and C. A. J. Ammerlaan, Phys. Rev. B **35**, 1566 (1987).
[11] K. L. Brower, Phys. Rev. B **4**, 1968 (1971).
[12] K. L. Brower, Phys. Rev. B **5**, 4274 (1972).
[13] S. H. Muller, Ph.D. thesis, University of Amsterdam, 1981.
[14] T. Gregorkiewicz, D. A. van Wezep, H. H. P. Th. Bekman, and C. A. J. Ammerlaan, Phys. Rev. Lett. **59**, 1702 (1987).
[15] E. G. Sieverts and C. A. J. Ammerlaan, in *Radiation Effects in Semiconductors, 1976* (Institute of Physics, Bristol, 1977), p. 213.
[16] E. G. Sieverts, Ph.D. thesis, University of Amsterdam, 1978.
[17] H. H. Woodbury and G. W. Ludwig, Phys. Rev. **117**, 102 (1960).
[18] G. H. Fuller, J. Phys. Chem. Ref. Data **5**, 835 (1976).
[19] J. R. Niklas and J. M. Spaeth, Phys. Status Solidi B **101**, 221 (1980).
[20] J. R. Morton and K. F. Preston, J. Magn. Reson. **30**, 577 (1978).
[21] D. R. Bosomworth, W. Hayes, A. R. L. Spray, and G. D. Watkins, Proc. R. Soc. London Ser. A **317**, 133 (1970).
[22] G. G. DeLeo, W. Beall Fowler, and G. D. Watkins, Phys. Rev. B **29**, 3193 (1984).
[23] S. Canuto and A. Fazzio, Phys. Rev. B **33**, 4432 (1986).
[24] C. A. J. Ammerlaan and J. C. Wolfrat, Phys. Status Solidi B **89**, 541 (1978).
[25] D. Ikenberry, A. N. Jette, and T. P. Das, Phys. Rev. B **1**, 2785 (1970).
[26] M. Lannoo, Phys. Rev. B **28**, 2403 (1983).
[27] M. Sprenger, Ph.D. thesis, University of Amsterdam, 1986.
[28] T. P. Das and E. L. Hahn, in *Nuclear Quadrupole Resonance Spectroscopy,* Suppl. 1 of *Solid State Physics,* edited by F. Seitz and D. Turnbull (Academic, New York, 1958).
[29] L. Pauling, *The Nature of the Chemical Bond,* 3rd ed. (Cornell University Press, Ithaca, NY, 1960), Chap. 3.